IEEE Photonics Journal
An IEEE Photonics Society Publication

Open Access

Photonics-Based Broadband RF Spectrum Measurement With Sliced Coherent Detection and Spectrum Stitching Technique

Volume 9, Number 5, October 2017

Guangyu Gao
Lihua Lei

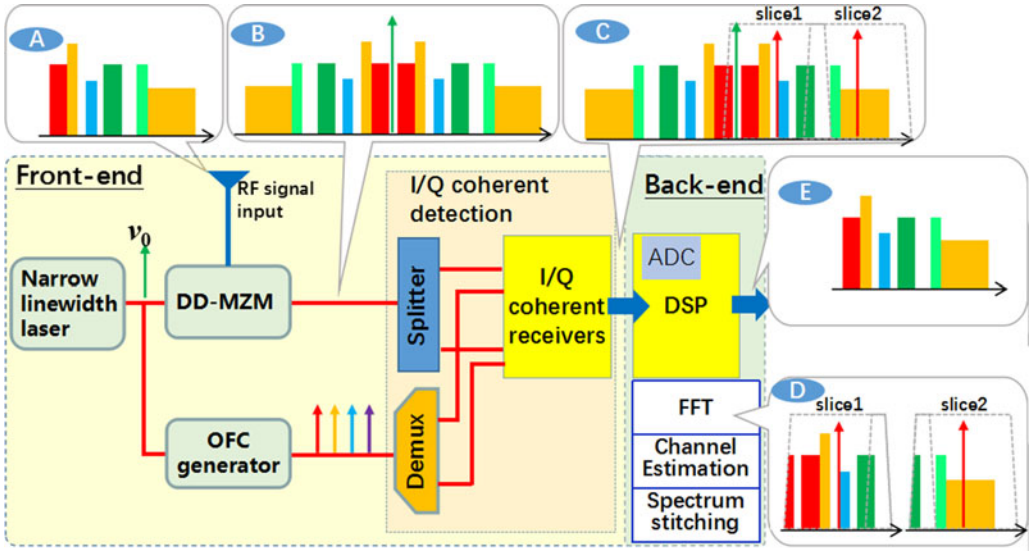

DOI: 10.1109/JPHOT.2017.2757609
1943-0655

Photonics-Based Broadband RF Spectrum Measurement With Sliced Coherent Detection and Spectrum Stitching Technique

Guangyu Gao and Lihua Lei

Qian Xuesen Laboratory of Space Technology, China Academy of Space Technology, Beijing 100094, China

DOI:10.1109/JPHOT.2017.2757609

Manuscript received July 11, 2017; revised September 13, 2017; accepted September 25, 2017. Date of publication September 28, 2017; date of current version October 9, 2017. This work was supported in part by the Independent Innovation Fund of Qian Xuesen Laboratory of Space Technology and in part by the Independent Research and Development Projects of China Aerospace Science and Technology Corporation. Corresponding author: Guangyu Gao (e-mail: gaoguangyu@qxslab.cn).
This paper has supplementary downloadable material available at http://ieeexplore.ieee.org.

Abstract: A novel photonics-based channelization approach is proposed for broadband radio frequency (RF) spectrum measurement with a single optical frequency comb, sliced coherent detection (SCD), and improved fast fourier transform-based digital signal processing. Through SCD, channel estimation and spectrum stitching, a broadband and complex RF spectrum can be detected and reconstructed with vector information in a high fidelity. A two-channel architecture as a proof of concept is characterized numerically with up to 40 GHz operation bandwidth, $\leq$12.5 GHz analysis bandwidth per channel, 113 dB·Hz$^{2/3}$ spurious free dynamic range, and 161 dB·Hz linear dynamic range. The potentials for further system developments in practice are also discussed.

Index Terms: Broadband radio frequency (RF) spectrum measurement, optical frequency comb, channelization, coherent detection, spectrum stitching.

1. Introduction

The broadband radio frequency (RF) spectrum measurement (BRSM) has drawn increasing interest in many applications, from wireless communications to electronic countermeasures [1]–[5]. As low frequency bands (LFB, lower than 6 GHz) become more and more crowded, new licensed frequencies have extended to over 30 GHz (in some applications even up to 100 GHz), promoting the RF measurement to cover higher bands. Meanwhile, there are pressing needs in improving the spectral efficiency on LFB with more effective spectrum monitoring capacities (i.e., spectrum sensing and sharing). Recently, a new conception to construct schemes by combining spectrum monitoring, management and control from a viewpoint of electromagnetic spectrum space is put forward, which is expected to integrate those typical RF applications over a broadband RF spectrum, such as communication, countermeasure, navigation and remote sensing [1], [2], [6]–[9]. Therefore, various and complex application scenarios drive BRSM towards higher frequencies and larger analysis bandwidths, which require enhanced capabilities for BRSM systems, including broader operating bandwidths (entire spectrum monitoring up to 40 GHz), higher frequency resolution,

real-time spectral analysis and higher dynamic range (DR). Relying on the advantages of photonic techniques in ultra-wide operating bandwidth, large instantaneous bandwidth, low loss, light weight, high-efficiency tunable filtering and local oscillator (LO), and intrinsic immunity to electromagnetic interference, many photonics-based RF measurement approaches [5], [10], [11], as next-generation solutions to overcome the limitations of traditional schemes with all-electric components, have been proposed and demonstrated in recent decades.

The channelization approaches are frequently used in photonics-based BRSM [2], [3], [12], [13], for their advantages in relatively high resolution, large optical instantaneous bandwidth and broadband measurements in parallel. Direct channelization is mostly preferred [7], [14]–[16], in which a broadband RF signal under detection is modulated on light, and sliced into many sub-channels by optical filters, then down-converted to baseband or intermediate frequency (IF) upon optical-electrical conversion in parallel. The final RF spectrum can be reconstructed by the direct power-frequency estimation at every channel without fast fourier transform (FFT) analysis. Although direct channelization is simple in signal processing, and has both ultrafast instantaneous frequency response (up to picosecond) in optical domain and ultra-wide operating bandwidth both in optical and electrical domain ($>$40 GHz), their performances are largely confined to several factors, such as the limited resolution of optical filter (usually $>$300 MHz), the difficulties in active alignment of optical carrier and filter, and the large number of channels. Direct channelization only produces a rough power spectrum of input signal without vector information, therefore it is not suitable for further signal analysis such as information interception in intelligence reconnaissance. Meanwhile, if the number of channels is at a high level, the BRSM structure will become quite complicated and cost, due to large amounts of transmission paths and receiving devices, even if photo-electricity integration techniques are introduced.

Recently, the combination of channelization, coherent detection and FFT-based DSP techniques comes up as a good performance and cost-effective solution with several advantages, such as low-level channelization scales, vector signal analysis, high frequency resolution and ultra-wide operation bandwidth [17]. Most of these approaches are based on dual-OFC and coherent detection. The RF signal under detection is modulated on one OFC, and copied to all of its coherent sub-carriers. Then the copies of the RF signal are channelized into small amounts of spectrum slices by regular optical filters. The spectrum slices are mixed with the other channelized OFC as LOs in optical hybrid, and fed into optical coherent receivers of corresponding channels to extract the in-phase (I) and quadrature (Q) components. After ADC sampling and DSP, the spectrum slices are down-converted to baseband or IF. The adoption of two coherent OFC guarantees stable and precise channelization without active optical carrier and filter alignment, and the numerical filter in DSP enables ideal amplitude/phase response in each channel and seamless covering over a broad band, avoiding the use of arrayed ultra-narrow tunable optical filters. Furthermore, FFT-based signal processing combined with coherent detection enables vector signal analysis of spectrum slices and provides high frequency resolution. However, there are still two major problems as well: on one hand, ultrahigh-repetition-rate and coherent dual-OFC are necessary in these approaches, which make BRSM systems very complicated and reduce the cost-effectiveness, for the generation of these types of dual-OFCs is difficult and cost high, either for coherent multi-sideband generation through electro-optical (EO) modulation, or for high-repetition-rate mode-locked laser; on the other hand, due to different spectrum slices only down-converted and analyzed in baseband or IF without capacities in the spectrum reconstruction of the entire RF spectrum, these approaches may have ambiguous ranges and are not suitable for global spectrum analysis in time domain and/or frequency domain.

In this paper, we propose a novel approach to realize a competitive photonics-based BRSM system with better practicability, completeness and cost-effectiveness based on a single OFC, low-level channelization, sliced coherent detection and improved FFT-based DSP. At the optical front-end, only a continuous wave (CW) light as optical carrier and a single OFC as optical LOs are employed instead of a coherent dual-OFC system. The single OFC using as optical LOs is generated by modulating the CW light with a single-frequency RF tone. The broadband RF spectrum under detection is modulated on the CW light instead of an OFC, and mixed with the LOs in optical hybrid

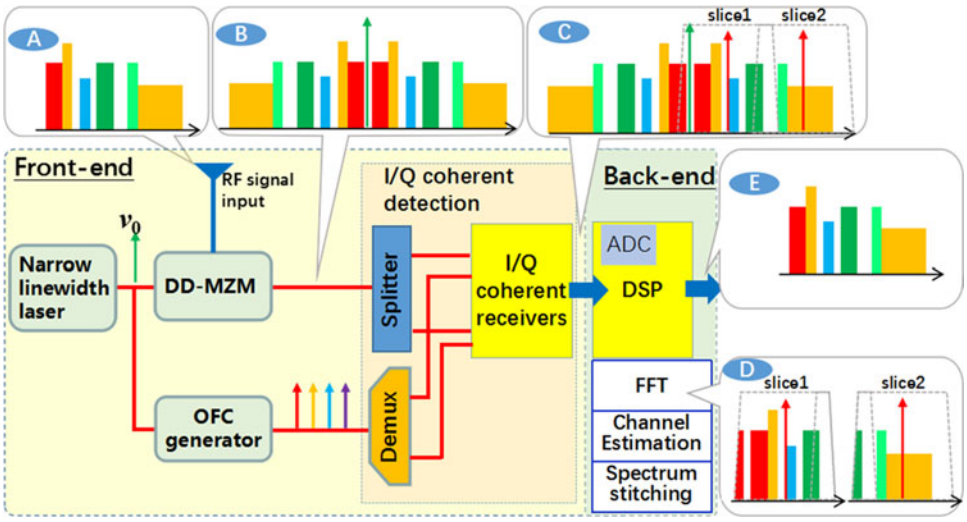

Fig. 1. The schematic of the proposed photonics-based BRSM system.

and received by coherent receivers to extract the I/Q components of different spectrum slices. The channelization of the modulated signal on light can be implemented in electrical domain by the direct down-conversion through optical coherent detection and the electrical low-pass filtering, removing the need of complex tunable optical filters and the active frequency alignment of the optical carriers. The coherence between CW light and OFC guarantees the stable and precise channelization and the spectrum stitching. At the electrical back-end, the entire RF spectrum can be reconstructed by DSP based on the I/Q components of different spectrum slices after numerical filtering, CE and spectrum stitching. As a proof of concept, a two-channel architecture is presented in simulation to demonstrate the abilities in detecting and reconstructing unknown broadband complex RF signal.

2. Principles

The schematic of the proposed photonics-based BRSM approach is shown in Fig. 1, comprised of two main parts, the optical front-end and the electrical back-end. In the front-end, a CW light at frequency v_0 from a narrow linewidth laser is divided into two paths by a power splitter, one path is sent to the OFC generator, and the other is sent to carry the RF signal under detection. In the OFC generator, the CW light is modulated to generate a single OFC in a dual-drive Mach-Zehnder modulator (DD-MZM) by double-sideband carrier-suppressed modulation (DSB-CS) with a CW RF tone at frequency f_{m}. By well setting the driving voltages and phase difference between the two RF-input paths of DD-MZM, an OFC with 6 flat and coherent comb lines at odd orders is generated, whose spacing equals to $2f_{\mathrm{m}}$. The remarkably suppressed lines at even orders can be further suppressed after optical demultiplexing, and can be neglected in the spectrum reconstruction processing. The small power ripple of the OFC has little impact on spectrum reconstruction, for it can be significantly compensated by spectral shaping in optical domain or in electrical domain with DSP. The frequencies of the comb lines are expressed as

$$f_{\mathrm{nth}} = v_0 + n \times 2f_m \tag{1}$$

$n \in [-3, 3]$ is the number of comb lines. The $+1$th and $+2$th lines of the comb are filtering out by an optical band-pass filter with center frequencies at $f_{+1\mathrm{th}} = v_0 + f_{\mathrm{m}}$ and $f_{+2\mathrm{th}} = v_0 + 2f_{\mathrm{m}}$. The CW light of the other path is modulated in another DD-MZM with the broadband RF signal under detection by DSB-CS. The modulation signal on light is divided into two paths by a power splitter, and fed into two I/Q receivers respectively to extract the I/Q components of the high-frequency sideband of the modulation signal in two channels by mixing and beating with the $+1$th and $+2$th comb lines.

The low-frequency sideband of the modulation signal can also be detected for BRSM by beating with the −1th and −2th lines of the OFC, but only one sideband is needed. The I/Q receivers are composed of a 90° optical hybrid, two balanced photodiodes (BPDs) and two output ports of I and Q paths. The channelization of this approach is not necessary to be implemented in optical domain with optical band-pass filters, but with low-pass filters (LPFs) in electrical domain for simplicity, provided that the number of the channelization is at a low level and little attention should be paid to the insertion loss of optical power splitters. The reason is that any spectrum slice of the modulated signal is easily down-converted to baseband by homodyne coherent detection with corresponding optical LOs and I/Q demodulation, and only half of the bandwidth of each spectrum slice should be sampled by ADC. Therefore, LPFs with a cutoff frequency f_{CH} at over a quarter of the broadband RF spectrum width can be employed as channelizers (also as anti-aliasing filters) before ADCs, to slice the broadband RF spectrum into two slices. And the process of multi-channel I/Q coherent detection with the electrical filtering is called after sliced coherent detection. After sampling and amplitude/phase calibration of the spectrum slices with CE, the channelization can further proceed with digitally rectangular filtering in frequency domain, enabling the spectrum stitching process as described in detail in following section.

In the back-end, the I/Q components of two channels are digitally processed by the DSP unit after sampling by ADC to reconstruct the entire broadband RF spectrum. The DSP unit consists of three procedures, the FFT, CE and spectrum stitching. By FFT with both of the I/Q components of each channel, the spectrum slices are reconstructed preliminarily in baseband, and the resulting slices are with some extent of spectrum distortion (SD). The SD mainly stems from the nonlinear response of the whole front-end links and can be compensated with CE in frequency domain. The principle of CE technique is described as follows. We assume that the RF signals at the input port of the front-end link and that at the output of the back-end have following relation

$$R(n) = A(n) H_{\text{link}}(n) + \varepsilon(n) \tag{2}$$

where $R(n)$, $A(n)$, $\varepsilon(n)$ and $H_{\text{link}}(n)$ are the expression in frequency domain of the received signal, the origin signal, the random noise and the response of the detection links. The maximum likelihood estimation of $H_{\text{link}}(n)$ can be expressed as

$$\hat{H}_{link}(n) = \frac{R(n)}{A(n)} = H_{\text{link}}(n) + \zeta(n) \tag{3}$$

where $\zeta(n)$ is the random noise. Since the response of the detection links is long-time-stable as compared to the fast time-variant characteristics of the broadband RF signal within the sampling windows, CE can be implemented with high-SNR estimation sequences within short-time gaps at a much lower rate than the refresh rate of BRSM. Thus $H_{\text{link}}(n)$ can be estimated according to (3) and taken as a long-time-stable value to deal with by averaging or smoothing, other than adopting complicated estimation algorithms. The estimation sequences can be implemented by broadband electrical multitones or broadband PRBS sequences generated respectively from electrical comb generators or high-speed pulse pattern generators (PPG). In these paper, a short-time and broadband sequence in the simulation system, comprised of ideal high-speed NRZ modulation signal added with Gaussian white noise, is employed as the channel estimation sequences. After CE process, both amplitude and phase of the reconstructed spectrum slices in two channel are calibrated.

Due to the coherence among the comb lines, adjacent spectrum slices are correlated with each other in phase and amplitude. Thus, the stitching values of adjacent slices can be estimated in amplitude and phase by

$$P_{\text{E}} = \arg\min \| P_{ch1}(i) - P_{ch2}(i) + P_{\text{E}} \|_2 \tag{4}$$

and

$$\theta_{\text{E}} = \arg\min \| \Delta\theta + \theta_{\text{E}} \|_2 \quad \text{s.t.} \quad \Delta\theta = \theta_{ch1}(i) - \theta_{ch2}(i) \quad \text{and} \quad \in [-\pi,\ \pi] \tag{5}$$

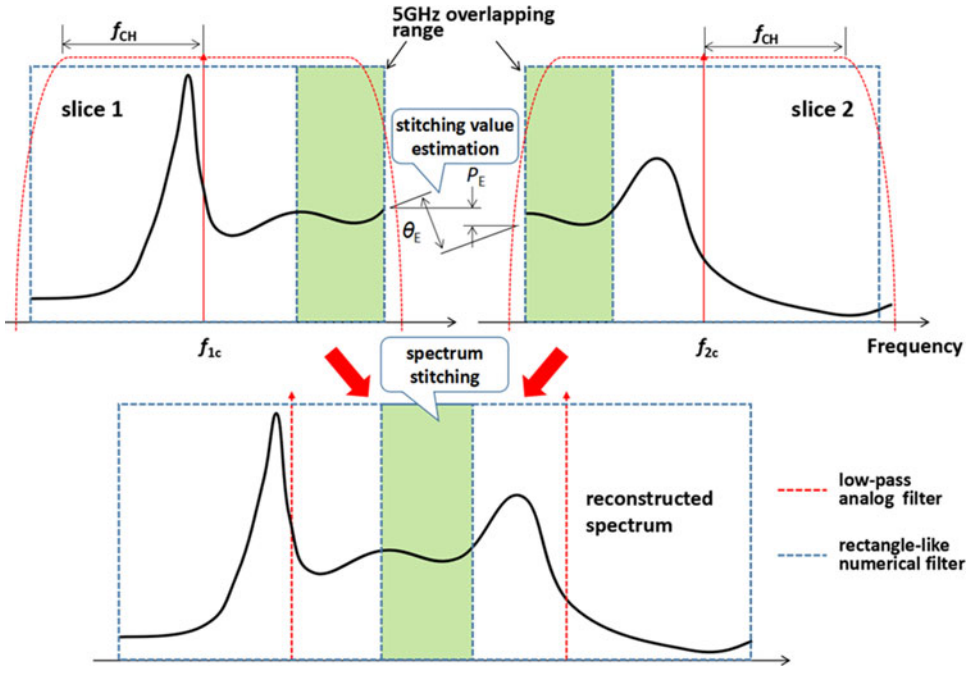

Fig. 2. Graphical representation of the spectrum stitching technique.

where i is the frequency position in the overlapping range of adjacent spectrum slices, P_E and θ_E are the estimated values of power difference in dB and phase difference in degree between adjacent slices. In the stitching process as shown in Fig. 2, the calibrated slices of different channels are first shifted to their origin frequency positions in the RF spectrum under detection, and then filtered by band-pass rectangle filters. The filters have linear phase response and bandwidths which are slightly larger than half of the operation bandwidth of BRSM, with center frequencies at f_{1c} and f_{2c} for the spectrum slices of channel 1 and 2. After frequency shift and filtering, the stitching values P_E and θ_E of adjacent slices are estimated through (4) and (5). Based on these values, the adjacent slices can be merged seamlessly in frequency domain. Accordingly, the entire broadband RF spectrum under detection will be reconstructed, and so is the waveform by IFT.

3. Results and discussion

The proof-of-concept simulation of a two-channel architecture as depicted in Fig. 1 is implemented with OptiSystem software to characterize the performance of the proposed approach. In the simulation, the optical power, carrier frequency and linewidth of the narrow linewidth laser is set at 16 dBm, 193.1 THz and 100 kHz. The DD-MZMs are set with parameters of half-wave voltages at 4 V, insertion losses at 5dB, extinction ratio at 30 dB, and modulation indices at 1.645 π for OFC generation and $<$0.12 π for RF-to-light modulation. In the OFC generator, the DD-MZM are modulated with a CW RF tone at 10 GHz by DSB-CS modulation to achieve an OFC with spacing at 20 GHz. The generated OFC is shown in Fig. 3, which has 6 comb lines with spacing of 20 GHz and flatness less than 1.5 dB. At the signal input part, the broadband RF signal under detection as shown in Fig. 4(a) is modulated onto the CW light in a DD-MZM by DSB-CS modulation. The spectral range of the broadband RF signal is 40 GHz, containing multi-signals generated from a self-made software module based on LabVIEW. The spectrum of the modulated signal on light is shown in Fig. 4(b), overlapped with the $+$1th and $+$2th comb lines serving as optical LOs of channel 1 and 2 respectively, representing that only the high-frequency sideband of the modulated signal on light is used to perform the direct down-conversion and channelization through coherent detection

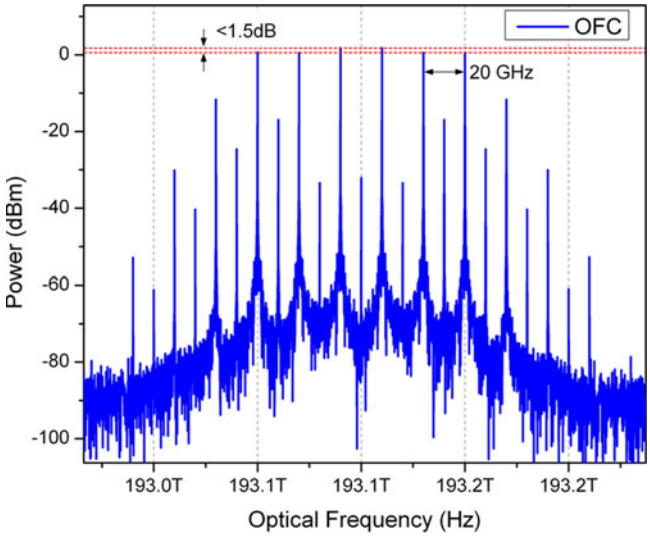

Fig. 3. Spectrum of the generated OFC.

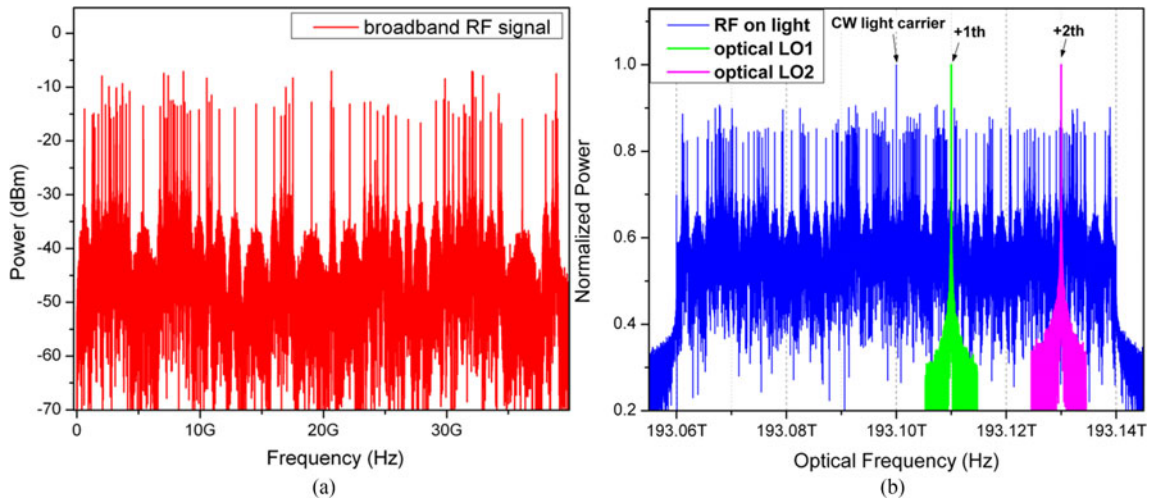

Fig. 4. The broadband RF signal under detection (a) and its spectrum (blue lines) modulated on light (b) with optical LOs of channel 1 (green line) and channel 2 (pink line).

and other subsequent procedures. It is feasible to filter the +1th and +2th comb lines from the OFC by optical filters in practice. For this two-channel architecture, optical band-pass filters with 12.5 GHz bandwidth and 50 dB depth (sufficient for BRSM and spectrum reconstruction) are available to achieve comb lines demultiplexing, such as Waveshaper and fiber Bragg gratings. Whereas for the architecture with more channels, high Q-factor filter arrays such as microring-based filters may be required when the comb spacing is too small to filter comb lines by regular optical filters.

The I/Q components of each channel after coherent detection are filtered by 4th low-pass Bessel filters with a cutoff frequency f_{CH} at 12 GHz for channelizing and anti-aliasing, and then sampled by ADCs with sampling rates at 25 GSa/s. The numeric signal of the I/Q components are transformed to frequency domain by FFT to perform preliminary spectrum reconstructions in baseband and further SD calibration with CE for each spectrum slice. The reconstructed spectrum of channel 1 and 2 after calibration are shifted to their origin frequency positions from baseband, and filtered by rectangle-like numeric filters with 25 GHz bandwidths and 10 GHz and 30 GHz center frequencies,

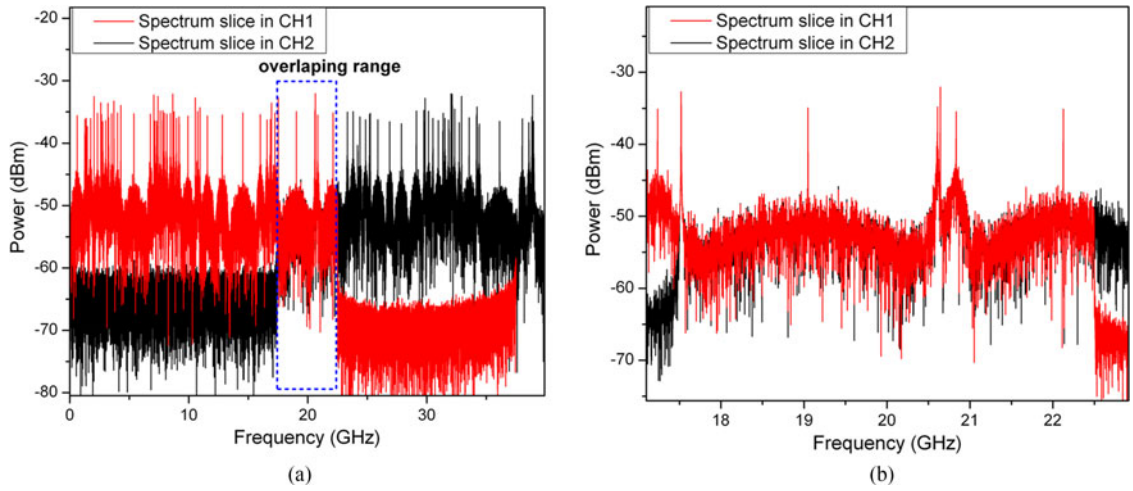

Fig. 5. (a) The reconstructed spectra of two channels in baseband with overlapping range from 17.5 GHz to 22.5 GHz: channel 1 (red) and channel 2 (black); (b) the detail of the overlapping range.

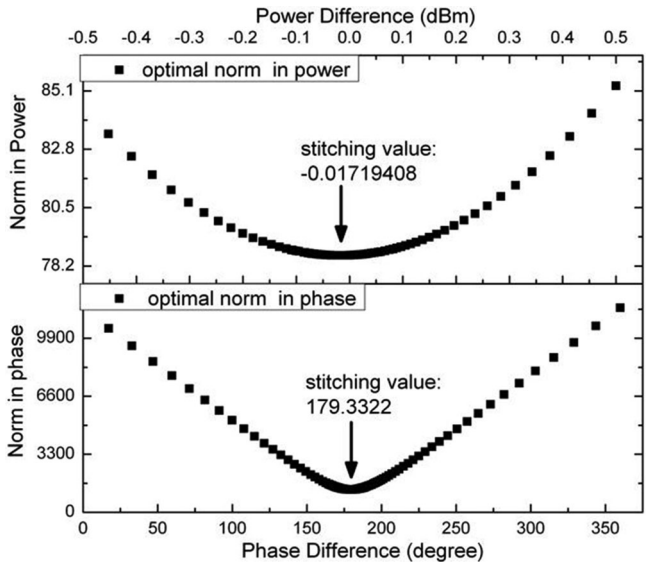

Fig. 6. The optimal estimation results of the stitching values and the estimation curves in power (upper curve) and phase (lower curve).

respectively. The resulting spectra of the two slices are shown in Fig. 5 (a), where 5 GHz overlapping ranges of them are marked with a blue dash-line rectangle and shown in detail in Fig. 5(b). From Fig. 5(b), the high-frequency range of channel 1 and the low-frequency range of channel 2 from 17.5 GHz to 22.5 GHz are perfectly overlapped with each other, representing nearly identical amplitude response. In order to stitching these two spectrum slices, the exact stitching values of amplitude and phase should be estimated with (4) and (5), in which the amplitude value is estimated in power with dBm and the phase is expressed with degree. The optimal estimated results of the stitching values and the estimation curves are shown Fig. 6, where the x and y axis of the upper part in Fig. 6 represent the estimated value and 2-norm of power differences between channel 1 and 2. And those of the lower part represent the estimated value and 2-norm of phase differences between channel 1 and 2. In the simulation setting, the actual stitching values should equal to

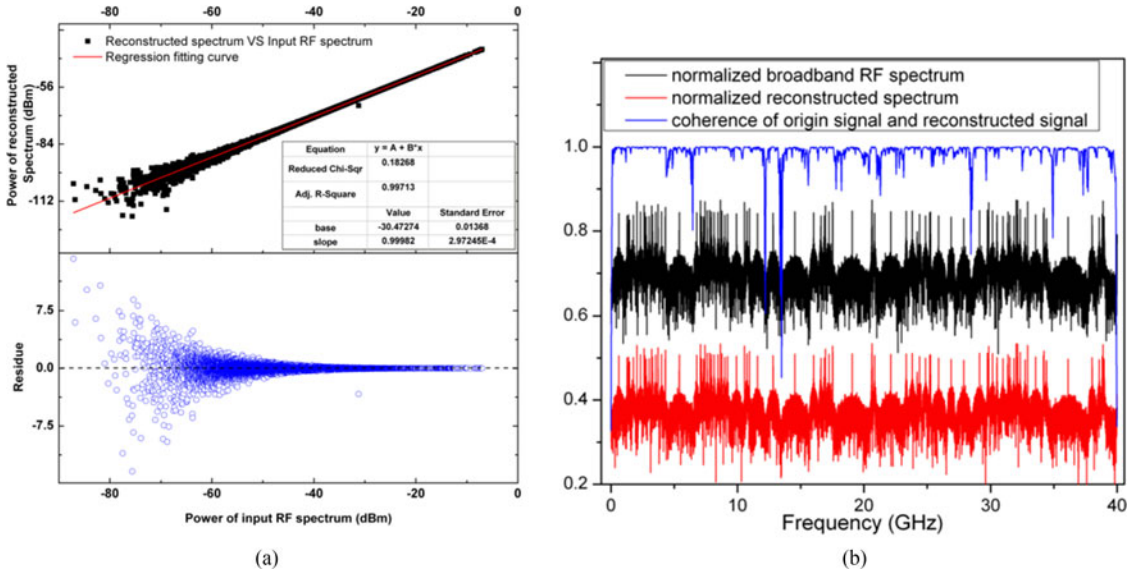

Fig. 7. (a) The linear regression analysis between the reconstructed spectrum and the broadband RF spectrum in frequency domain, upper: power distribution, lower: power deviation of output signal to the linear fitting curve; (b) The coherence between the restored waveform of the reconstructed spectrum and that of the broadband RF spectrum.

0 dBm and 180 degree, whereas the noise influences on the detection signals from the front and back end and the errors from CE result in small deviations of the estimated values from the real ones. However, the small deviations are within the acceptable level and have little impact on the results of spectrum reconstruction, as shown in Fig. 7.

The linear regression analysis in frequency domain between the reconstructed spectrum and the input RF spectrum is depicted in Fig. 7(a) to characterize the performance of the spectrum reconstruction, where the upper part is the power distribution of the output signal versus the input signal, and the lower part is the power deviation of the output signal versus the linear fitting curve. The power distribution appears to be high linearity, and can be well fitted with a linear curve with base at -30.5 dBm and slope at ~ 1 @3e-4 standard error as listed in the inset table of Fig. 7(a), indicating the input RF spectrum under detection is reconstructed with high fidelity, and the system is working in the linear region for the input RF signal as shown in Fig. 4(a). The power deviation gives the information about the extent to which the detected output power is different from the ideal value. As shown in the lower part of Fig. 7(a), the power deviations are negligible at the frequency points with high input power. But as input power decreasing to some extent, the power deviation becomes observable gradually. For example, when the input power is lower than -60 dBm, the power deviations occur at more than ± 3 dB (with a deviation ratio at $\pm 3.3\%$ as compared to the expected output power at -90 dBm). The increasing power deviation at the frequency points with low input power indicates the interference from the noise floor, which determines the detection sensitivity. The performance of the spectrum reconstruction in time domain is also characterized by the coherent analysis between the waveforms of the reconstructed spectrum and the input RF spectrum as shown in Fig. 7(b), where the normalized curves of the input RF spectrum and the reconstructed spectrum are also depicted below the coherence curve showing negligible differences. The coherence analysis provides the information about the linear extent of an I/O system, and here it is used to estimate the correlation characteristic between the input signal and output signal and which frequency components will lose more information after detection and reconstruction. In Fig. 7(b), the coherence degree for most of frequency points is close to 1, especially for the frequency points with relatively high input power, revealing high fidelity to the waveform reconstruction of the input signal. Only those frequency points with low input power, which

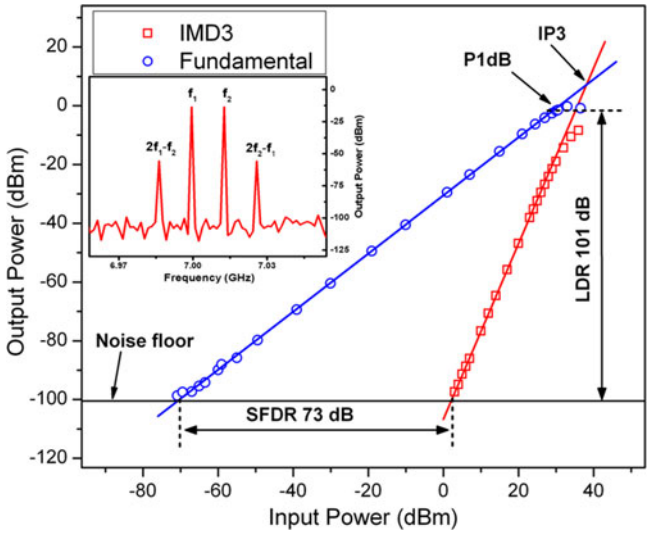

Fig. 8. The performance characterization of the linear dynamic range and spurious free dynamic range. The output power of fundamental signal (blue) and the IM3 signal (red) versus the input power.

are susceptible significantly to the interference of noise floor as also shown in Fig. 7(a), present observable deterioration in coherence degree. Good performance in waveform reconstruction can also be confirmed with linear regression analysis between the input and output waveforms, which is shown in fig 1s in the supplement information.

The system performances are also characterized in terms of dynamic range and linearity as shown in Fig. 8. Two RF tones at 7.00 GHz and 7.01 GHz, with input power varying from -80 to 36 dBm, are used to measure the linear response and the third-order inter-modulation product (IMD3). The power of the RF tones at the input ports of the DD-MZM is measured as the input power, and the power of corresponding frequencies in the reconstructed spectrum is measured as the output power. The fundamental and the third harmonic signal power are plotted against the input RF power in Fig. 8. The resolution bandwidth (RBW) is 1.2 MHz (0.8 μs sampling widow for FFT), the noise floor occurs at -101.5 dBm, and the minimum detectable signal of the fundamental and the third harmonic components are -71 dBm and 2 dBm at the input ports. The measured spurious free dynamic range (SFDR) is 73 dB (113 dB·Hz$^{2/3}$), and the linear dynamic range (LDR) of the fundamental component is measured at 101 dB (161 dB·Hz) with 1 dB-compression point (P1dB) at 30 dBm for input power. The SFDR and LDR results have $>$6 dB·Hz$^{2/3}$ and 20 dB·Hz performance improvements respectively in comparison with those in [18], [19]. The high linearity of the fundamental component is consistent with the result of the linear regression analysis between the reconstructed spectrum and the input RF spectrum as shown in Fig. 7(a), further confirming the BRSM system worked at the linearity region with reliable capacities in spectrum reconstruction. Please note that, the LDR and SFDR results of the two-channel architecture in the simulation are based on a setting of high performance ADCs which have perfect SFDR and effective number of bits (ENOB). Whereas for a practical system, the measured LDR and SFDR should be limited to real-world ADCs to some extent. According to the relation between ENOB and signal-to-noise-plus-distortion ratio (SNDR) in [20], the required ENOB is calculated to be $<$7.5 bit for a 101dB LDR. As for SFDR, commercial high-speed ADCs with SFDR higher than 60 dB and ENOB $>$7 bit are available for this proof-of-concept architecture and further higher-performance produces are on the way. Thus, the limitations from ADC to the measured LDR and SFDR are not significant for this proposed approach.

Although the results discussed above are only based on a proof of concept of a two-channel architecture, a practical BRSM system based on this proposed approach with a moderate

channelization level and better performance is achievable in consideration of the trade-off among the channelization level, the hardware/software requirement and the system performance. Channelization in a moderate level can not only extend the RF spectrum under detection to a wider range, for example it is feasible to detect a ultra-wide band RF spectrum with up to 100 GHz bandwidth based on nearly infinite-wide frequency coverage of coherent optical LOs and the forthcoming high-bandwidth EO modulator; but also will greatly enhance the performances, such as frequency resolution, SFDR and LDR by decreasing the noise floor through relatively narrower analysis bandwidth and smaller RWB; and will increase the cost-effectiveness by reducing the requirements for high-speed hardware and power dissipation.

4. Conclusion

A novel photonics-based channelization approach is proposed to realize a competitive BRSM system with better practicability, completeness and cost-effectiveness based on a single OFC, low-level channelization, sliced coherent detection and improved FFT-based DSP. Relying on the coherence of the spectrum slices and the DSP algorithm including CE and spectrum stitching, a broadband and complex RF spectrum can be detected and reconstructed in a high fidelity. A proof of concept of a two-channel architecture is analyzed in simulation to demonstrate the abilities in detecting and reconstructing the broadband and complex RF spectrum. The operation bandwidth is up to 40 GHz, and the analysis bandwidth per channel is $\leq$12.5 GHz. Good performances of the BRSM system in spectrum detection and reconstruction are characterized and discussed by regression analysis, coherence analysis, dynamic range and linearity analysis (SFDR, 113 dB·Hz$^{2/3}$ and LDR, 161 dB·Hz) between the reconstructed signal and the input signal. This proposed approach also possesses potentials for further system developments in practice, including extended operation bandwidth, better frequency resolution, better SFDR and LDR, and better cost-effectiveness.

Acknowledgment

The authors would like to acknowledge Dr. Naijin Liu and Dr. Jianjun Zhang for the helpful discussions.

References

[1] J. B. Tsui, *Digital Techniques for Wideband Receivers*, 2th ed. New Delhi, India: SciTech Publishing, 2004.
[2] S. Pan and J. Yao, "Photonics-based broadband microwave measurement," *J. Light. Technol.*, vol. 35, no. 16, pp. 3498–3513, Aug. 2016.
[3] X. Zou, B. Lu, W. Pan, L. Yan, A. St??hr, and J. Yao, "Photonics for microwave measurements," *Laser Photon. Rev.*, vol. 10, no. 5. pp. 711–734, Sep. 2016.
[4] W. Wang *et al.*, "Characterization of a coherent optical RF channelizer based on a diffraction grating," *IEEE Trans. Microw. Theory Tech.*, vol. 49, no. 10, pp. 1996–2001, Oct. 2001.
[5] H. Emami, M. Ashourian, and M. Ebnali-Heidari, "Dynamically reconfigurable all optical frequency measurement system," *J. Light. Technol.*, vol. 32, no. 24, pp. 4194–4200, Dec. 2014.
[6] X. Yang *et al.*, "Optical frequency comb based multi-band microwave frequency conversion for satellite applications," *Opt. Exp.*, vol. 22, no. 1, p. 869, 2014.
[7] X. Xie *et al.*, "Broadband photonic radio-frequency channelization based on a 39-GHz optical frequency comb," *IEEE Photon. Technol. Lett.*, vol. 24, no. 8, pp. 661–663, Apr. 2012.
[8] W. Qihui and R. Jing, "New paradigm of electromagnetic spectrum space: spectrum situation," *J. Nanjing Univ. Aeronaut. Astronaut.*, vol. 48, no. 5, pp. 625–633, 2016.
[9] M. P. Fitz, T. R. Halford, I. Hossain, and S. W. Enserink, "Towards simultaneous radar and spectral sensing," in *Proc. IEEE Int. Symp. Dyn. Spectrum Access Netw.*, 2014, pp. 15–19.
[10] R. Li *et al.*, "Optical serial coherent analyzer of radio-frequency (OSCAR)," *Opt. Exp.*, vol. 22, no. 11, pp. 13579–13585, 2014.
[11] S. T. Winnall and A. C. Lindsay, "A Fabry-Perot scanning receiver for microwave signal processing," *IEEE Trans. Microw. Theory Tech.*, vol. 47, no. 7, pp. 1385–1390, Jul. 1999.
[12] H. Chen *et al.*, "Photonics-assisted serial channelized radio-frequency measurement system with nyquist-bandwidth detection," *IEEE Photon. J.*, vol. 6, no. 6, Dec. 2014, Art. no. 7903707.
[13] Y. Dai *et al.*, "Broadband photonic radio frequency (RF) channelization based on coherent optical frequency combs and polarization I/Q demodulation," *Sci. China Technol. Sci.*, vol. 56, no. 3, pp. 621–628, 2013.

[14] X. Zou, W. Pan, B. Luo, and L. Yan, "Photonic approach for multiple-frequency-component measurement using spectrally sliced incoherent source," *Opt. Lett.*, vol. 35, no. 3, pp. 438–440, 2010.
[15] Z. Li, X. Zhang, H. Chi, S. Zheng, X. Jin, and J. Yao, "A reconfigurable microwave photonic channelized receiver based on dense wavelength division multiplexing using an optical comb," *Opt. Commun.*, vol. 285, pp. 2311–2315, 2012.
[16] C. Wang and J. P. Yao, "Ultrahigh-resolution photonic-assisted microwave frequency identification based on temporal channelization," *IEEE Trans. Microw. Theory Tech.*, vol. 61, no. 12, pp. 4275–4282, Dec. 2013.
[17] X. Xie *et al.*, "Broadband photonic RF channelization based on coherent optical frequency combs and I/Q demodulators," *IEEE Photon. J.*, vol. 4, no. 4, pp. 1196–1202, Aug. 2012.
[18] D. Onori *et al.*, "A direct-conversion RF scanning receiver based on photonics," in *Proc. IEEE MTT-S Int. Microw. Symp. Dig.*, 2016, pp. 2–5.
[19] W. Wang *et al.*, "Characterization of a coherent optical RF channelizer based on a diffraction grating," *IEEE Trans. Microw. Theory Tech.*, vol. 49, no. 10, pp. 1996–2001, Oct. 2001.
[20] C. Laperle and M. Osullivan, "Advances in high-speed DACs, ADCs, and DSP for optical coherent transceivers," *J. Light. Technol.*, vol. 32, no. 4, pp. 629–643, Feb. 2014.